CRYSTAL GROWTH & DESIGN

pubs.acs.org/crystal

Article

Color Polymorphs of ROY-ol

Bernardo A. Nogueira,* Susana M. M. Lopes, Alberto Milani, Vânia André, José A. Paixão, M. Ermelinda S. Eusébio, Teresa M. V. D. Pinho e Melo, M. Teresa Duarte, Chiara Castiglioni, and Rui Fausto

Cite This: *Cryst. Growth Des.* 2022, 22, 5375−5389

Read Online

ACCESS | Metrics & More | Article Recommendations | Supporting Information

ABSTRACT: Color polymorphism is a fascinating property exhibited by compounds that have polymorphs of different colors. The most famous family of substances forming molecular organic color polymorphs is the ROY family of compounds. ROY, which states for the red, orange, and yellow colors of the polymorphs of 5-methyl-2-((2-nitrophenyl)amino)thiophene-3-carbonitrile, is currently the compound exhibiting the largest number of known polymorphs (12), all of them with crystallographic structures determined. In this study, the color polymorphism exhibited by a novel member of the ROY family, 2-((4-hydroxy-2-nitrophenyl)-amino)thiophene-3-carbonitrile (ROY-ol), has been investigated. Four color polymorphs of ROY-ol were identified (one bright-burgundy and the others dark-burgundy), from which the crystal structures of two (polymorphs 1 and 2) were solved by single-crystal X-ray diffraction, and the intermolecular interactions in these crystals being subsequently evaluated using the Hirshfeld analysis method. These two polymorphs were also characterized vibrationally by infrared and Raman spectroscopies, supported by fully periodic density functional theory (DFT) calculations. The performed thermal analysis studies, undertaken by differential scanning calorimetry (DSC), polarized light thermomicroscopy (PLTM), and temperature-variation Raman spectroscopy, allowed us to identify two additional polymorphs of ROY-ol (polymorphs 3 and 4). Investigation of the conformational space of the ROY-ol isolated molecule within the DFT framework (together with similar calculations on similar molecules, including ROY) allowed to establish a series of correlations between the conformational landscapes of the molecules and some relevant characteristics of the polymorphism the compounds exhibit. As a whole, a detailed description of the color polymorphism exhibited by ROY-ol has been achieved, which is an additional contribution to the understanding of this phenomenon.

1. INTRODUCTION

Color polymorphism is an interesting property of chemical systems that present polymorphs with different colors.[1] Despite the potential applications for these systems as time−temperature sensors and photoelectronic devices with multiplex capabilities, for example,[2−5] there are only a few families of compounds that have the ability to form molecular organic color polymorphs. One of the most famous is the ROY family of compounds. ROY, first described in 1995,[6] is the common designation of 5-methyl-2-((2-nitrophenyl)amino)thiophene-3-carbonitrile (Scheme 1a), which states for the red, orange, and yellow colors of its polymorphs. ROY is currently the compound exhibiting the largest number of known polymorphs (12), and the crystallographic structures of all of them have already been determined.[6−12]

The different colors of the ROY polymorphs have been attributed mainly to structural variations associated with the conformational flexibility around the N−$C_{(thiophene)}$ bond (θ in Scheme 1), which determines the relative orientation of the two rings present in the molecule (phenyl and thiophene) that, in turn, determines the extent of the π-electron delocalization in the molecule. Interestingly, the red and orange polymorphs were

Scheme 1. Molecules of ROY (a), AcROY (b), and ROY-ol (d)

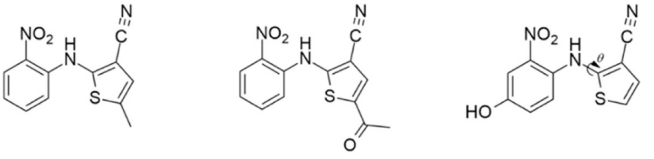

a ROY b AcROY c ROY-ol

Received: April 19, 2022
Revised: August 6, 2022
Published: August 18, 2022

https://doi.org/10.1021/acs.cgd.2c00462
Cryst. Growth Des. 2022, 22, 5375−5389

found to be formed by one of the conformers of the molecule (where the two rings are closer to co-planarity), while the yellow polymorphs are formed by a different conformer. Nevertheless, at least one of the yellow polymorphs of the compound is constituted by the conformer present in the red and orange forms, so that ROY is a chemical system that exhibits both conformation- and packing-determined color polymorphism.[1]

More recently, other compounds of the ROY family have been reported to also present polymorphs of different colors, such as 2-((2-nitrophenyl)amino)thiophene-3-carbonitrile, also showing red, orange, and yellow polymorphs,[13] 5-methyl-2-((4-methyl-2-nitro-phenyl)amino)thioph-ene-3-carbonitrile, which had three different red polymorphs (of different tones) and one orange polymorph identified,[14] 2,2′-((ethyne-1,2-diylbis(2-nitro-4,1-phenylene))bis(azanediyl))bis(5-methylthiophene-3-carbonitrile) (or simply el-ROY), with three identified polymorphs, with red and orange shades,[15] and 2-((2-nitrophenyl)amino)furan-3-carbonitrile (FuROY), for which three polymorphs were structurally characterized, one orange-yellow, one red, and one orange-red.[16] Earlier this year, we synthesized a new derivative of ROY, 5-methyl-2-((4-methyl-2-nitro-phenyl)amino)thiophene-3-carbonitrile, which we named AcROY (Scheme 1b), and that presents orange, yellow, and burgundy polymorphs.[17]

In the present study, the color polymorphism exhibited by the newest member of the ROY family, 2-((4-hydroxy-2-nitrophenyl)amino)thiophene-3-carbonitrile (Scheme 1c), or ROY-ol, was investigated. Compared to ROY, ROY-ol lacks the methyl group on the thiophene ring and presents a hydroxyl group in a meta position in relation to the nitro group of the nitrophenyl ring. The compound was prepared in a three-step synthetic route and characterized by ^{1}H and ^{13}C NMR spectroscopy, melting point determination, infrared spectroscopy, and high-resolution mass spectrometry with electrospray ionization (HRMS-ESI). Polymorph screening was then performed by the slow-evaporation recrystallization method, using a large number of solvents with different characteristics, which rendered two color polymorphs (one bright-burgundy and the other dark-burgundy). The structures of the two polymorphs were determined by single-crystal X-ray diffraction (XRD), and the polymorphs were also characterized vibrationally by both infrared and Raman spectroscopies, supported by fully periodic density functional theory (DFT) calculations. The dominant intermolecular interactions in the crystals were evaluated using the Hirshfeld analysis method. Finally, the thermal analysis of the compound was undertaken by differential scanning calorimetry (DSC), polarized light thermomicroscopy (PLTM), and temperature-variation Raman spectroscopy. From these studies, two additional polymorphs of ROY-ol were discovered. In the last section of this article, DFT calculations undertaken for the isolated ROY-ol molecule are presented and used together with similar calculations on ROY and AcROY molecules to establish a series of correlations between the conformational landscapes of the molecules and some relevant characteristics of the polymorphism they exhibit.

2. MATERIALS AND METHODS

2.1. Synthesis and Instrumental Methods. ROY-ol was synthesized in a three-step sequence (Scheme 2). First, the hydroxyl group of the commercially available 4-fluoro-3-nitrophenol (**1**) was protected with a benzyl group by reaction with benzyl bromide in the presence of a base, affording compound **2** in a high yield. The nucleophilic aromatic substitution reaction between compound **2** and

Scheme 2. Synthetic Strategy to ROY-ol

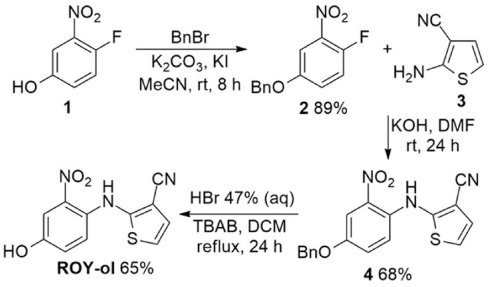

2-aminothiophene-3-carbonitrile (**3**) gave compound **4** in a 68% yield. Finally, ROY-ol was obtained in a 65% yield by cleavage of the benzyl group using HBr 47% (aq) in refluxing dichloromethane.

*2.1.1. Synthesis of 4-Benzyloxy-1-fluoro-2-nitrobenzene (**2**).* Potassium carbonate (6 mmol, 0.829 g) and catalytic potassium iodide (4 mg) were added to a solution of 4-fluoro-3-nitrophenol (**1**) (4 mmol, 0.628 g) and benzyl bromide (4.4 mmol, 0.532 mL) in acetonitrile (25 mL). The reaction mixture was stirred at room temperature for 8 h. After this time, ethyl acetate (25 mL) was added, and the mixture was washed with water (2 × 25 mL) and brine (25 mL), dried, and the solvent evaporated off. The compound was obtained as a white solid (3.58 mmol, 89%) by crystallization from petroleum ether, filtered, and dried under vacuum. M.p. 85.4−86.9 °C. IR (attenuated total reflection (ATR)) ν 746, 834, 1007, 1222, 1319, 1350, 1493 and 1535 cm^{-1}. ^{1}H NMR δ ($CDCl_3$): 5.10 (s, 2H), 7.17−7.23 (m, 3H), 7.35−7.43 (m, 5H), 7.61−7.63 (m, 1H). ^{13}C NMR δ ($CDCl_3$): 71.1, 110.7 (d, J = 2.7 Hz), 119.1 (d, J = 22.6 Hz), 122.9 (d, J = 7.7 Hz), 127.6, 128.5, 128.8, 135.5, 137.2 (d, J = 8.4 Hz) 150.2 (d, J = 258.7 Hz), 154.5 (d, J = 2.6 Hz). HRMS (ESI) m/z for $C_{13}H_9NO_3F$ [M − H$^+$] calcd 246.0572, found 246.0575.

*2.1.2. Synthesis of 2-((4-Benzyloxy-2-nitrophenyl)amino)-thiophene-3-carbonitrile (**4**).* A solution of 2-aminothiophene-3-carbonitrile (**3**) (2 mmol, 0.248 g) and 4-benzyloxy-1-fluoro-2-nitrobenzene (**2**) (2 mmol, 0.495 g) in dimethylformamide (14 mL) was added dropwise to a suspension of KOH (3 mmol, 0.168 g) in dimethylformamide (6 mL). After the addition was complete, the reaction mixture was stirred at room temperature for 6 h, an additional portion of KOH (1 mmol, 0.056 g) was added at once, and the reaction mixture was stirred for another 16 h. The reaction mixture was poured into a mixture of water/ice and extracted with dichloromethane (3 × 30 mL). The combined organic phases were washed with HCl 1 M (2 × 30 mL) and brine (2 × 20 mL), dried, and the solvent evaporated off. The compound was obtained as a red solid (1.36 mmol, 68%) by crystallization from ethanol, filtered, and dried under vacuum. M.p. 134.2−135.7 °C. IR (ATR) ν 752, 1007, 1142, 1222, 1262, 1524, 1588 and 2213 cm^{-1}. ^{1}H NMR δ ($CDCl_3$): 5.09 (s, 2H), 6.99 (d, J = 5.6 Hz, 1H), 7.08 (d, J = 5.6 Hz, 1H), 7.26 (dd, J = 9.2 and 3.2 Hz, 1H), 7.31 (d, J = 9.2 Hz, 1H), 7.35−7.38 (m, 1H), 7.39−7.45 (m, 4H), 7.80 (d, J = 2.8 Hz, 1H), 9.63 (s, 1H). ^{13}C NMR δ ($CDCl_3$): 70.9, 102.0, 109.7, 113.9, 118.0, 119.1, 126.8, 127.7, 128.4, 128.8, 134.7, 135.8, 152.3, 152.9. HRMS (ESI) m/z for $C_{18}H_{14}N_3O_3S$ [M + H$^+$] calcd 352.0750, found 352.0744.

2.1.3. Synthesis of 2-((4-Hydroxy-2-nitrophenyl)amino)-thiophene-3-carbonitrile (ROY-ol). HBr 47% aq (3 mL) and tetrabutylammonium bromide (0.036 mmol, 11.4 mg) were added to a solution of compound **4** (0.142 mmol, 50 mg) in dichloromethane (5 mL). The reaction mixture was stirred under reflux for 24 h. After this time, the mixture was diluted with dichloromethane (20 mL), washed with water (2 × 20 mL) and brine (20 mL), dried, and the solvent evaporated off. The crude product was purified by flash chromatography [ethyl acetate/hexane (1:2)] giving compound ROY-ol as an orange solid (0.093 mmol, 65%). M.p. 167.9−169.1 °C (from $CHCl_3$). IR (ATR) ν 798, 950, 1142, 1217, 1403, 1517, 1593, 2218, 3269 and 3354 cm^{-1}. ^{1}H NMR δ (dimethyl sulfoxide (DMSO)-d_6): 7.06 (d, J = 6.0 Hz, 1H), 7.13 (d, J = 6.0 Hz, 1H), 7.16 (dd, J = 8.8 and 2.8 Hz, 1H), 7.25 (d, J = 8.8 Hz, 1H), 7.43 (d, J = 2.8 Hz, 1H), 9.45 (s, 1H), 10.16 (br

https://doi.org/10.1021/acs.cgd.2c00462
Cryst. Growth Des. 2022, 22, 5375−5389

s, 1H). ^{13}C NMR δ (DMSO-d_6): 94.7, 110.6, 114.9, 116.7, 123.6, 126.5, 130.1, 139.3, 153.0, 158.3. HRMS (ESI) m/z for $C_{11}H_8N_3O_3S$ [M + H^+] calcd 262.0281, found 262.0279.

The synthesized compounds were initially characterized by ^{1}H and ^{13}C NMR and infrared (IR) spectroscopy (Figures S1−S6, Supporting Information), as well as high-resolution mass spectra (HRMS) and melting point determination. The NMR spectra were recorded on a Bruker Avance III instrument operating at 400 MHz (^{1}H) or 100 MHz (^{13}C). The solvents used were deuterochloroform ($CDCl_3$) or hexadeuterodimethyl sulfoxide (DMSO-d_6). The IR spectra were collected in the attenuated total reflection (ATR) mode in an Agilent Cary 630 FT-IR Fourier transform spectrometer, with a diamond-based ATR cell (Smart Orbit). HRMS experiments were done by electrospray ionization (ESI) in an orbitrap q-exactive focus mass spectrometer. Melting point (uncorrected) was determined in an open glass capillary.

The polymorph screening was performed by slow-evaporation recrystallization (5−25 mg), at room temperature, using different solvents (4−20 mL).

Single-crystal X-ray diffraction (XRD) determinations were performed at room temperature in a Bruker APEX II diffractometer, using graphite monochromated Mo Kα (λ = 0.71073 Å) radiation. The structures were solved by the dual-space algorithm implemented in SHELXT-2018/2,[18] and full-matrix least-squares refinement of the structural model was performed using SHELXL-2018/3.[19] All non-hydrogen atoms were refined anisotropically. All hydrogen atoms except those of the hydroxyl and amine groups were placed at calculated idealized positions and refined as riding using SHELXL-2018/3 default values.[19] The hydroxyl and amine hydrogen atoms were refined isotropically with a displacement parameter constrained to 1.5× (hydroxyl) or 1.2× (amine) of the U_{iso} value of the parent atom. Full details of the data collection and structure refinement are given in the Supporting Information (Crystallographic Data). A summary of the data collection and refinement is provided in Table 1. The CIF files containing the supporting crystallographic data for the two polymorphs of ROY-ol were deposited at the Cambridge Crystallographic Data Centre, with the references CCDC 2160983 (polymorph-1) and CCDC 2160984 (polymorph-2).

The IR spectra (400−4000 cm^{-1} wavenumber region; spectral resolution 1 cm^{-1}; 512 accumulations) of the purified polymorphs were obtained in a Thermo Scientific FT-IR Nicolet iS5 system, using an iD7 ATR accessory with a diamond crystal (incidence angle: 45°). The Raman spectra were obtained in a Raman Horiba LabRam HR Evolution Raman system, using a HeNe laser as an excitation source (633 nm) with an approximate power of 0.5 mW at the sample, to prevent photodegradation. Calibration was done using a silicon crystal wafer (reference peak: 520.5 cm^{-1}). The spot area of the laser was approximately 100 μm^2, which was focused on the sample through a 50× long working distance objective. The final spectra were the average of 500 accumulations of individual spectra collected during 1 s, with a spectral resolution of 0.5 cm^{-1}.

The differential scanning calorimetry (DSC) experiments were performed in a PerkinElmer Pyris-1 power compensation calorimeter, equipped with a 1:1 v/v ethylene glycol/water cooler (−25 °C) and a 20 mL min^{-1} nitrogen purge flow. Aluminum pans (hermetically sealed) were used (sample weight: 0.8−2 mg), with an empty pan used as the reference. The temperature and enthalpy calibrations were done using indium (PerkinElmer, 99.99%, T_{fus} = 156.6 °C; $\Delta_{fus}H_m$ = 3286 ± 13 J mol^{-1}) and caffeine (Mettler Toledo, ME 18872, T_{fus} = 235.6 ± 0.2 °C). The samples were scanned from 25 to 200 °C (scan rate: 10 °C min^{-1}). Polarized light thermal microscopy (PLTM) analyses were performed using a Linkam DSC600 hot stage, with a Leica DMRB microscope and a Sony CCD-IRIS/RGB video camera. Images at 50× magnification were collected by combined use of polarizers and wave compensators and occasionally using crossed polarizers. The samples were heated at a rate of 10 °C min^{-1}, from 25 to 200 °C.

2.2. Computational Details. The DFT calculations on isolated molecules, including geometry optimizations and calculations of the potential energy profiles, were carried out using Gaussian 09 (version D.01).[20] The three-parameter B3LYP functional, which includes Becke's gradient exchange correction[21] and the Lee, Yang, and Parr correlation functional,[22] was used together with the 6-311++G(2d,p) basis set.[23]

Fully periodic calculations on the crystalline structures were performed using the CRYSTAL17 code[24,25] and include geometries and cell parameter optimizations as well as calculation of infrared and Raman spectra (at the Γ point, by the diagonalization of the numerically calculated Hessian matrices) of the ROY-ol polymorphs. The input structures were experimentally determined in this work by XRD. The calculations were performed within the DFT theoretical framework with the PBE0 functional[26] and the 6-31G(d,p) basis set.[27] Calculated frequencies were scaled by the factor 0.9512,[28] to allow a better comparison with the experimental data.

Table 1. Summary of the Single-Crystal X-ray Data Collections and Crystal Structure Refinements

	polymorph-1	polymorph-2
chemical formula	$C_{11}H_{17}N_3O_3S$	$C_{11}H_{17}N_3O_3S$
formula weight	261.26	261.26
color, shape	bright-burgundy/ plate	dark-burgundy/ block
space group	$P2_1/n$	$P2_1/n$
temperature (K)	292(2)	293(2)
cell volume (Å^3)	1129.0(6)	2265.9(3)
crystal system	monoclinic	monoclinic
a (Å)	7.867(2)	8.6557(7)
b (Å)	13.046(3)	12.9351(12)
c (Å)	11.519(4)	20.2404(18)
α (deg)	90	90
β (deg)	107.26(3)	90.806(4)
γ (deg)	90	90
Z,Z'	4,1	8,2
D_c (Mg m^{-3})	1.537	1.532
radiation (Å) (graphite; monochromated)	0.71073	0.71073
max. crystal dimensions (mm)	0.23 × 0.20 × 0.08	0.06 × 0.04 × 0.04
θ range (deg)	2.422−27.493	2.546−27.499
range of h, k, l	−10, 10; −16, 16; −14, 14	−11, 11; −16, 16; −26, 26
reflections measured/ independent	70 874/2602	68 321/5211
reflections observed ($I > 2\sigma$)	1873	3161
data/restraints/parameters	2602/0/169	5211/0/338
GOF	1.053	1.020
R_1 ($I > 2\sigma$)	0.0375	0.0574
wR_2	0.1087	0.1619
function minimized	$\sum w(\lvert F_o\rvert^2 - S\lvert F_c\rvert^2)$	$\sum w(\lvert F_o\rvert^2 - S\lvert F_c\rvert^2)$
diff. density final max/min (e Å^{-3})	0.174, −0.264	0.266, −0.350

3. RESULTS AND DISCUSSION

3.1. Polymorph Screening and IR and Raman Band Marks of the Polymorphs 1 and 2 of ROY-ol. The synthesized ROY-ol material was subjected to polymorph screening through recrystallization from different solvents using the solvent room-temperature slow-evaporation technique. The solvents used included apolar, polar-aprotic, and polar-protic solvents. Two different polymorphs exhibiting different colors were identified (Figure 1; see also Figure S7 in the Supporting Information): polymorph-1 (bright-burgundy), which was obtained from recrystallization in methanol (together with polymorph-2), and polymorph-2 (dark-burgundy), which was found upon recrystallization in all used solvents (mixed with polymorph-1 in the case of recrystallization from methanol).

The identity of the polymorphs was first confirmed by IR-ATR and Raman spectroscopies. The spectra of the two

https://doi.org/10.1021/acs.cgd.2c00462
Cryst. Growth Des. 2022, 22, 5375−5389

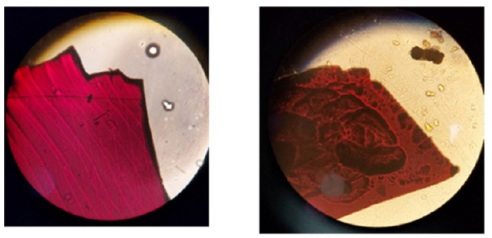

Figure 1. ROY-ol polymorphs 1 (left) and 2 (right). Images are amplified 50×.

polymorphs are shown in Figure 2 and present clear distinct profiles. Marker bands for fast differentiation of the two polymorphs could be identified. In the IR spectra, polymorph-1 exhibits intense bands at 1584, 1506, and 1339 cm^{-1}, whereas in polymorph-2, the corresponding bands are observed at 1592, 1516, and 1356 cm^{-1}, respectively. Noteworthy, the spectral signature of the C≡N stretching mode is clearly different for the two polymorphs. In the IR spectrum of polymorph-1, this mode gives rise to a single band at 2228 cm^{-1}, while in the case of polymorph-2, a doublet of bands at 2224 and 2218 cm^{-1} is observed. Additionally, the 3500−2900 cm^{-1} spectral region (where the bands due to the CH, NH, and OH stretching vibrations are observed) is also clearly distinctive for both polymorphs, as seen in Figure 2. In the Raman spectra, the most intense peak appears at the same frequency (816 cm^{-1}) in the spectra of both polymorphs. However, characteristic Raman bands of polymorph-1 are observed at 1277, 1265, and 1150 cm^{-1}, while in the spectrum of polymorph-2, band marks are observed at 1239, 1210, and 1142 cm^{-1}. The Raman spectra of the two polymorphs are particularly distinguishable in the 1000−1600 cm^{-1}, the region where the Raman bands in the spectrum of polymorph-2 are considerably more intense than those in the Raman spectrum of polymorph-1 (Figure 2).

To better understand the vibrational features in both the IR and Raman spectra of polymorphs 1 and 2 of ROY-ol, fully periodic DFT calculations were performed for these two crystalline structures. These involved the crystallographic structure optimization and the calculation of the correspondent vibrational spectra at the PBE0/6-31G(d,p) level of theory. The experimentally observed and calculated vibrational frequencies are provided in Tables S1 and S2, while the calculated spectra are compared with the experimental ones in Figures S8 and S9.

The calculations show a good general agreement with the experimental data and allowed a characterization of the above-mentioned marker bands. Hence, the calculations indicate that the IR marker bands of polymorph-1 observed at 1584, 1506, and 1339 cm^{-1} correspond to the antisymmetric stretching mode of the NO_2 moiety, a CC stretching vibration delocalized throughout the two rings of the molecule, and a CC stretching localized mode of the thiophene ring, respectively. In turn, the IR marker bands of polymorph-2 observed at 1592, 1516, and 1356 cm^{-1} are assigned to the NO_2 antisymmetric stretching mode, to the same CC stretching vibration delocalized throughout the two rings of the molecule that in polymorph-1 is observed at 1506 cm^{-1}, and to a vibration containing large contributions of both the OH and NH bending modes. On the other hand, Raman marker bands of polymorph-1 observed at 1277, 1265, and 1150 cm^{-1} correspond to a mixed NH/OH bending vibration and two different CH bending modes of the nitrophenyl ring. These bands have counterparts in the Raman marker bands of polymorph-2 observed at 1239, 1210, and 1142 cm^{-1}.

3.2. Crystal Structure of the Polymorphs 1 and 2 of ROY-ol and Hirshfeld Surface Analysis. The X-ray crystallographic studies determined that the two polymorphs of ROY-ol crystalize in the monoclinic system, $P2_1/n$ (no. 14) space group, with a = 7.867(2) Å, b = 13.046(3) Å, c = 11.519(4) Å, β = 107.26(3)°, V = 1129.0(6) $Å^3$, Z = 4, and Z' = 1 for polymorph-1 and a = 8.6557(7) Å, b = 12.9351(12) Å, c = 20.2404(18) Å, β = 90.806(4)°, V = 2265.9(3) $Å^3$, Z = 8, and Z' = 2 for polymorph-2. Thus, polymorph-2 distinguishes from polymorph-1 in that the unit cell has twice the volume of polymorph-1 and accommodates two symmetry-independent molecules in the unit cell. In addition, as described below, the molecular conformation of the molecules in the two polymorphs differs significantly, as well as the hydrogen-bonding scheme responsible for cohesion of the structures in the crystalline state.

Figure 3 depicts the molecular geometry found in the crystals of the two polymorphs, where, in both cases, the OH substituent of the nitrophenyl ring and the cyano substituent of the

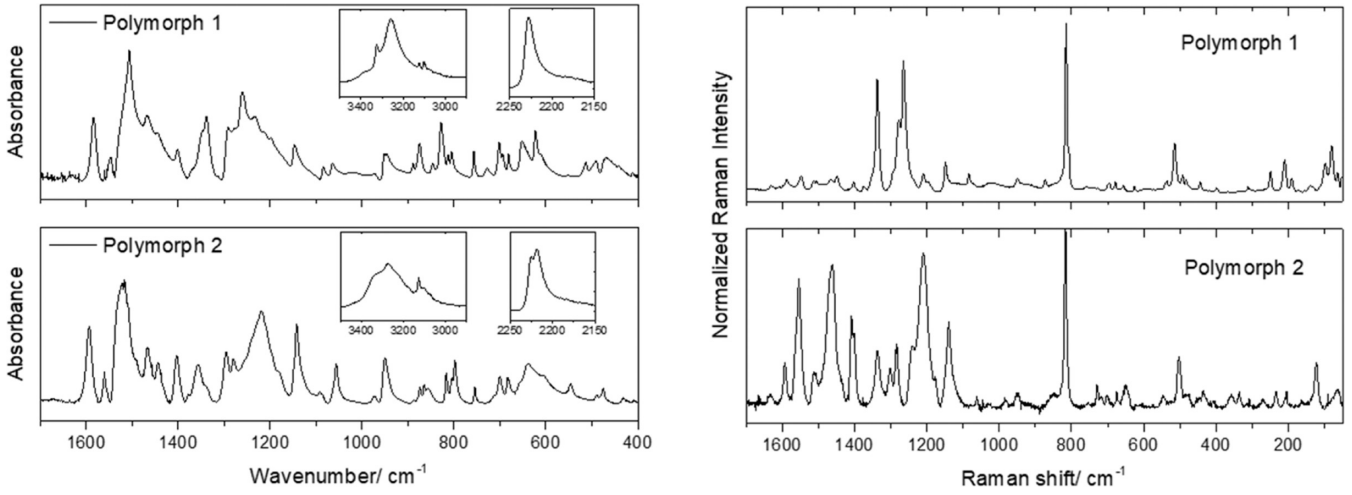

Figure 2. IR (left) and Raman (right) spectra of polymorphs 1 and 2 of ROY-ol, respectively, in the 400−1700 cm^{-1} wavenumber and 50−1700 cm^{-1} Raman shift range.

https://doi.org/10.1021/acs.cgd.2c00462
Cryst. Growth Des. 2022, 22, 5375−5389

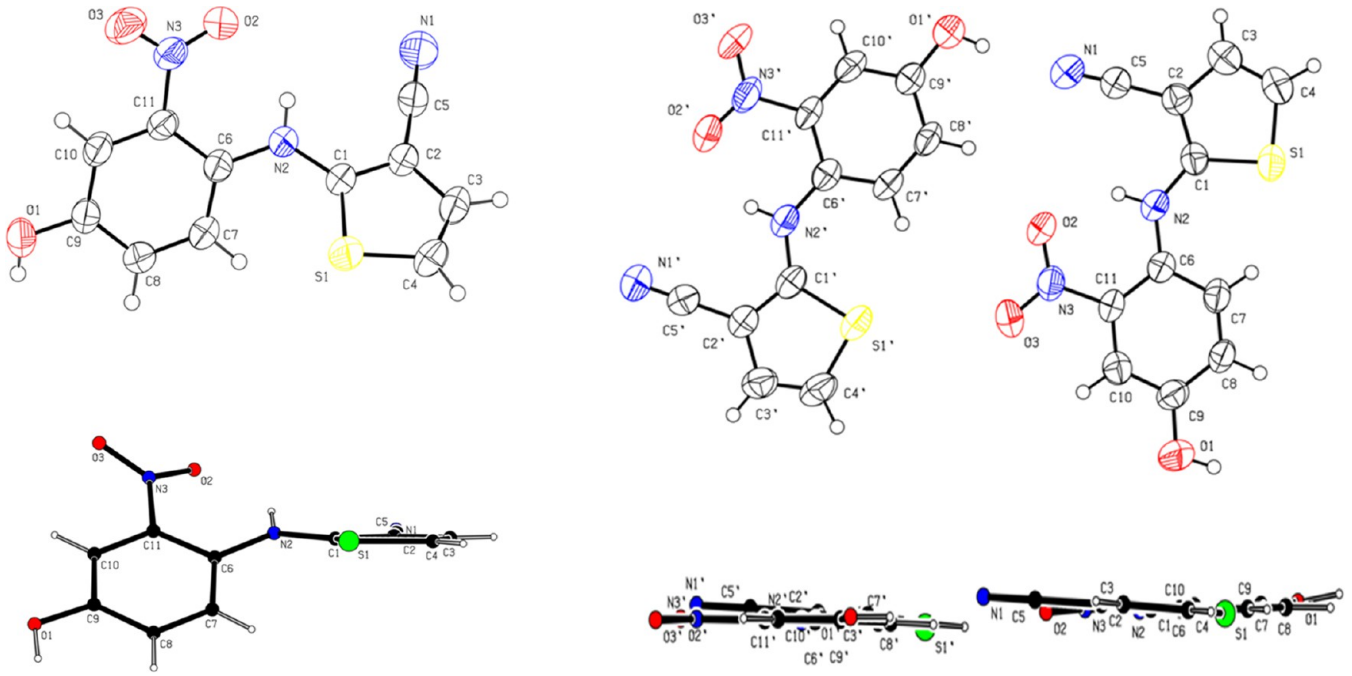

Figure 3. Oak Ridge Thermal Ellipsoid Plot (ORTEP) plots depicting the anisotropic displacement ellipsoids drawn at the 50% probability level and the atom numbering schemes for polymorph-1 (left) and polymorph-2 (right). In the bottom panel, a profile view of the molecules is shown (viewing direction parallel to the thiophene ring plane).

thiophene ring point away from and toward the nitro group, respectively.

In both polymorphs, a strong intramolecular hydrogen bond is present between the amine N−H group and an O atom from the neighbor nitro group acting as a proton acceptor. It is notorious that both symmetry-independent molecules present in the unit cell of polymorph-2 are almost strictly planar, with torsion angles around the rotational degrees of freedom present in the molecule being close to 0/180°, the C−N−C−S dihedral angle being −6.7(5)° in one of the molecules and 7.9(5)° in the other. In contrast, the molecule in polymorph-1 is found to have a significant deviation from planarity, with the C−N−C−S dihedral angle being −31.6(3)°. In polymorph-1, the nitro group is also significantly tilted (23.1(2)°) from the plane of the phenyl ring (see Figure 3). Bond lengths and valence angles are similar in the two polymorphs and fall within the range of values observed in similar compounds.(Tables 2 and 3)[1,5−17]

Molecular packing and the associated set of intermolecular interactions are distinct in the two polymorphs, even if in both

Table 2. Valence Angles (deg) in the Thiophene and Nitrophenyl Rings of Polymorphs 1 and 2 of ROY-ol

angle	polymorph-1	polymorph-2
C1−C2−C3	112.92(18)	114.1(3)/113.6(3)
C2−C3−C4	112.16(18)	111.4(3)/111.7(3)
C3−C4−S1	112.85(15)	113.4(3)/113.6(3)
C4−S1−C1	91.46(10)	91.62(16)/91.74(17)
S1−C1−C2	110.56(14)	109.5(2)/109.5(2)
C6−C7−C8	122.01(17)	121.9(3)/122.8(3)
C7−C8−C9	120.70(18)	123.1(3)/121.6(3)
C8−C9−C10	118.93(18)	116.9(3)/118.1(3)
C9−C10−C11	120.07(17)	120.4(3)/120.7(3)
C10−C11−C6	122.34(17)	122.4(3)/121.9(3)
C11−C6−C7	115.92(17)	115.4(3)/114.9(3)

Table 3. Relevant Dihedral and Torsion Angles (deg) for Polymorphs 1 and 2 of ROY-ol

dihedral/torsion angle	polymorph-1	polymorph-2
∠(C1···S1)/(C6−C11)	46.52(7)	4.2(2)/4.4(2)
∠(C6···C11)/N3O2O3	23.1(2)	0.8(6)/1.8(6)
C6−C11−N3−O2	24.0(3)	−1.3(5)/−0.3(5)
C6−C11−N3−O3	−157.6(2)	179.0(3)/178.6(3)
C6−N2−C1−S1	−31.6(3)	−6.7(5)/7.9(5)
C1−N2−C6−C11	156.9(2)	−177.3(3)/177.2(3)
C6−N2−C1−C2	155.4(2)	174.9(3)/−174.5(3)

the major role is played by a strong N−H···O hydrogen bond between the cyano and hydroxyl groups of neighbor molecules. In polymorph-1, these hydrogen bonds interconnect the molecules forming chains running parallel to the crystallographic *b*-axis. Parallel sets of chains are further weakly linked by nonclassic C−H···O hydrogen bonds between the thiophene rings and the hydroxyl groups, forming an extensive hydrogen-bond network, as depicted in Figure 4. In polymorph-2, the N−H···O hydrogen bond between the cyano and hydroxyl groups is established between the two symmetry-independent molecules, forming chains running along the [110] and [1$\bar{1}$0] crystallographic directions and, in addition, a weaker C−H···O interaction between a C−H group of the phenyl ring and the O2 atom that participates as well in the intramolecular N−H···O bond is also present. These chains are further interlinked by weaker C−H···O between the thiophene rings and the hydroxyl groups, as depicted in Figure 5. Notoriously, one of the O atoms of the nitro group does not participate in the hydrogen-bond network in either of the polymorphs. Inspection of the short contacts present in the two polymorphs discloses a more extensive set for polymorph-2 (Table 4). In polymorph-1, only one such contact adds to those of the hydrogen bonds discussed above, which occurs between the S atom and the H atom of a

https://doi.org/10.1021/acs.cgd.2c00462
Cryst. Growth Des. 2022, 22, 5375−5389

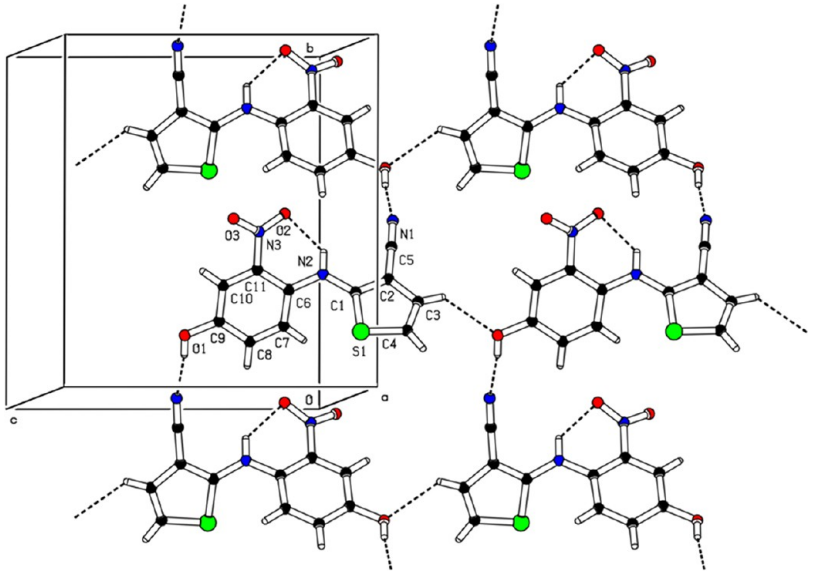

Figure 4. Hydrogen-bonding network in polymorph-1 of ROY-ol showing the 1D chains running along the crystallographic direction *b*-axis with molecules joined by strong N−H···O hydrogen bonds. These chains are linked to identical chains in the unit cell via weaker C−H···O hydrogen bonds. For clarity, not all molecules present in the unit cell are shown.

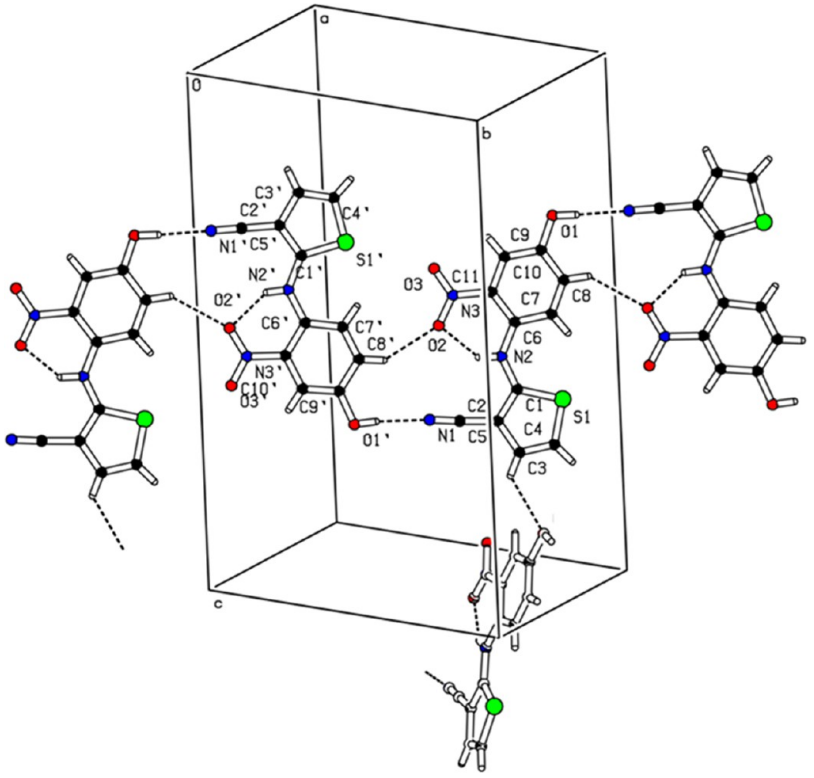

Figure 5. Hydrogen-bonding network in polymorph-2 of ROY-ol showing the 1D chains running along the [110] and [1$\bar{1}$0] crystallographic directions joined by strong N−H···O hydrogen bonds. These chains are interlinked via weaker C−H···O hydrogen bonds. For clarity, not all molecules present in the unit cell are shown, only one chain running along [110] and the interconnection to a single molecule of another chain that runs along [1$\bar{1}$0] are depicted.

close C−H group of the nitrophenyl ring (a similar C−H···S intramolecular contact is also present in polymorph-2).

To characterize in detail the dominant intermolecular interactions in the crystals of polymorphs 1 and 2 or ROY-ol, the Hirshfeld surface analysis method developed by Spackman and co-workers was used.[29,30] The analyses were done using Crystal Explorer 17.5,[31] using as input the crystal structures obtained in the XRD studies.

Maps of the normalized contact distance, d_{norm}, on the calculated Hirshfeld surfaces and the respective 2D fingerprint plots were obtained (Figures 6 and S10−S12 in the Supporting Information). d_{norm} is calculated from the distances to the surface of the nearest atom outside, d_e, and inside, d_i, the surface,

https://doi.org/10.1021/acs.cgd.2c00462
Cryst. Growth Des. 2022, 22, 5375−5389

Table 4. Hydrogen Bonds and Short Intermolecular Contact Distances and Angles for Polymorphs 1 and 2 of ROY-ol[a]

D−H···A	D−H	H−A	D···A	∠D−H···A
polymorph-1				
O1−H1···N1[b]	0.79(3)	1.98(3)	2.769(3)	170(3)
N2−H2···O2	0.82(3)	2.03(2)	2.653(2)	132(2)
C3−H3···O1[c]	0.93	2.50	3.184(3)	130.4
C7−H7···S1	0.93	2.73	3.220(2)	113.6
polymorph-2				
O1−H1···N1[d]	0.89(5)	1.99(5)	2.874(4)	177(5)
N2−H2···O2	0.86(4)	1.90(4)	2.597(4)	137(3)
C3−H3···O1′[e]	0.93	2.49	3.157(4)	128.6
C7−H7···S1	0.93	2.47	3.194(3)	134.3
C8−H3···O2′[d]	0.93	2.51	3.295(4)	142.4
N2′−H2′···N3′	0.82(4)	2.49(4)	2.922(4)	114(3)
N2′−H2′···O2′	0.82(4)	1.91(4)	2.608(3)	142(3)
C4′−H4′···O1	0.93	2.65	3.412(4)	139.3
C7′−H7′···S1′	0.93	2.43	3.156(3)	135.3
C8′−H8′···O2	0.93	2.43	3.233(4)	144.3
O1′−H1′···N1	0.82(5)	2.01(5)	2.816(4)	170(5)

[a]Distances and angles are given in Å and degrees, respectively. [b]Symmetry codes: $3/2 - x, -1/2 + y, 1/2 - z$. [c]$x, y, -1 + z$. [d]$1 + x, 1 + y, z$. [e]$1/2 - x, 1/2 + y, 3/2 - z$.

as defined in the eq 1, where r^{vdW} is the van der Waals radii of the atoms.

$$d_{norm} = \frac{d_i - r_i^{vdW}}{r_i^{vdW}} + \frac{d_e - r_e^{vdW}}{r_e^{vdW}} \quad (1)$$

The d_{norm} maps allow the identification of the regions of the molecule in the crystal where intermolecular interactions are more relevant,[30,32] while the 2D fingerprint plots summarize the information about the relative importance of the different types of contacts (combinations of d_e and d_i, expressed as percentages of the surface area allocated to each combination of atoms) throughout the Hirshfeld surface of the molecule (Table 5).[33−35]

Figure 6 shows the maps of d_{norm} on the Hirshfeld surfaces of the crystallographic asymmetric units of polymorphs 1 and 2 of ROY-ol, showing also the neighboring molecules, which account for the strongest interactions (shorter contacts, indicated by the red spots on the Hirshfeld surfaces). The d_{norm} values vary from −0.646 to 1.361 in polymorph-1 and from −0.573 to 1.327 in polymorph-2. For polymorph-1, the shortest intermolecular contacts are related to the H-bonds established between the OH substituent of the nitrophenyl moiety and the N atom of the cyano substituent of the thiophene ring, while the second most relevant intermolecular interactions are associated with the weak nonclassical H-bonds formed between the thiophene ring (through the *m*-hydrogen atom) and the oxygen atom of the hydroxyl group. In the case of the polymorph-2, while the most important interactions between the two molecules that constitute the asymmetric unit of the crystal involve the OH group and the cyano N atom, on one side, and the oxygen atoms of the nitro group and the hydrogen atom of the nitrophenyl group in p-position to the NO_2 moiety, on the other side (see Figure S10 in the Supporting Information), the most important interactions between the asymmetric unit of the crystal as a whole and the adjacent molecules are similar to those existing in polymorph-1 (see Figure 6): (i) the H-bond interactions established by the OH groups and the cyano N atoms that do not participate in the intermolecular H-bond interaction inside the asymmetric unit dimer (which are established, respectively, with the cyano N atom and the OH group of adjacent molecules) and (ii) weak nonclassical H-bonds formed between thiophene rings (through the *m*-hydrogen atom) of neighboring molecules and the oxygen atom of the hydroxyl groups of the molecules forming the asymmetric unit dimer (and vice versa).

Table 5 displays the percentages of the Hirshfeld surfaces assigned to the different types of contacts (d_e vs d_i), which are also shown graphically in the 2D fingerprint d_e vs d_i plots provided in the Supporting Information (Figures S11 and S12). H···O/O···H contacts are prevalent in both polymorphs, representing 23.2 and 25.6% of the total surface areas of polymorphs 1 and 2, respectively, when for polymorph-2, the full asymmetric unit is considered, and is mostly related to the C−H···O nonclassical hydrogen-bond interactions referred to above. When the individual molecules in the asymmetric unit of polymorph-2 are considered, the percentage of the total surface area assigned to the H···O/O···H contacts increases, as expected, because between the two molecules, one of the dominant interactions involves the oxygen atoms of the nitro group and the hydrogen atom of the nitrophenyl group in p-position to the NO_2 moiety, as mentioned above. The second and third most relevant types of contacts are the H···H contacts (18.4 and 16.2% in polymorphs 1 and 2, respectively; somewhat lower, i.e., 14.5% on average, if individual molecules in the unit cell of polymorph-2 are considered), which are associated to intermolecular interactions of dispersive type, and the H···N/N···H contacts (14.1 and 11.8%), which are essentially related to the strong O−H···N hydrogen-bond interactions established

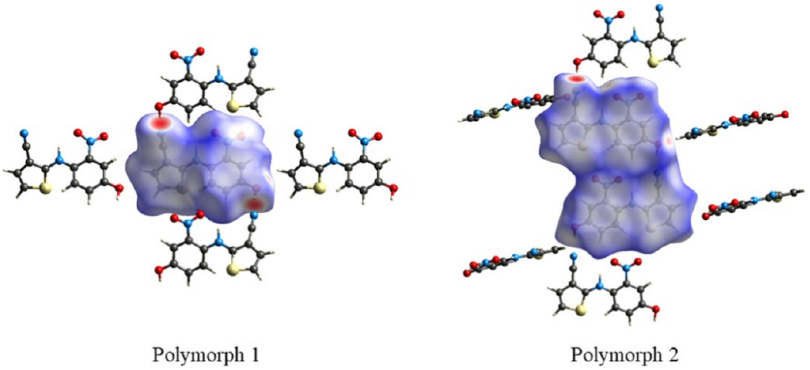

Figure 6. Maps of d_{norm} on the Hirshfeld surfaces of the crystallographic asymmetric units of polymorphs 1 (left) and 2 (right) of ROY-ol, showing also the neighboring molecules, which account for the strongest interactions (shorter contacts).

https://doi.org/10.1021/acs.cgd.2c00462
Cryst. Growth Des. 2022, 22, 5375−5389

Table 5. Fractional Areas (in %) of the Hirshfeld Surface Assigned to the Different Intermolecular Contacts in ROY-ol Polymorphs 1 and 2

		polymorph-2			
intermolecular contact	polymorph-1 asymmetric unit ($Z' = 1$)	asymmetric unit ($Z' = 2$)	independent molecule 1	independent molecule 2	independent molecules average
H···O/O···H	23.2	25.6	26.4	28.6	27.5
H···H	18.4	16.2	13.7	15.2	14.5
H···N/N···H	14.1	11.8	14.0	16.3	15.2
C···C	10.6	10.4	9.5	9.4	9.5
H···C/C···H	8.2	13.3	12.2	11.3	11.8
H···S/S···H	5.4	3.2	2.9	3.4	3.2
C···N/N···C	5.2	3.7	3.2	3.3	3.3
O···S/S···O	5.1	1.3	2.4	2.8	2.6
N···O/O···N	3.7	3.4	4.0	2.0	3.0
C···O/O···C	3.4	3.6	3.5	2.8	3.2
C···S/S···C	1.1	4.6	6.0	2.4	4.2
O···O	0.9	0.6	0.6	0.5	0.6
N···S/S···N	0.6	1.2	0.9	1.2	1.1
S···S	0.1	0.0	0.0	0.0	0.0
N···N	0.0	0.9	0.7	0.8	0.8

between the OH groups and the cyano N atoms (also as expected considering the O−H···N interaction within the two molecules of the asymmetric unit of polymorph-2, the H···N/N···H contact percentage increases to 15.2% in average when the individual molecules are taken in separate). Interestingly, the most significant difference between the major intermolecular interactions in the crystals of the polymorphs 1 and 2 of ROY-ol is observed for the H···C/C···H contacts, which correspond to 8.2% of the surface area in polymorph-1 and to almost twice this value (13.3%) in polymorph-2 (11.8% in average when the two molecules of its asymmetric unit are taken in separate). In polymorph-1, the close H···C/C···H contacts are related to the parallel stacking of the nitrophenyl and thiophene rings of adjacent molecules (i.e., nitrophenyl···thiophene stacking interactions), while in the case of polymorph-2, these contacts result from parallel stacking between the same type of the ring in adjacent molecules (i.e., nitrophenyl···nitrophenyl and thiophene···thiophene ring staking interactions). The sum of the areas related to the principal hydrogen-bond intermolecular interactions (H···O/O···H, H···N/N···H, and H···S/S···H) is 42.7% for polymorph-1 and 45.9% (average values for the two independent molecules) for polymorph-2, which suggest that H-bonding might be globally more relevant in the packing of polymorph-2 than in polymorph-1.

3.3. Thermal Studies (DSC, PLTM, and Temperature-Dependent Raman Spectroscopy). The thermal behavior of ROY-ol polymorphs 1 and 2 was first investigated by DSC. Since it was not possible to isolate the sufficient amount of polymorph-1 to conduct an experiment with this polymorph alone (polymorph-1 always co-forms with polymorph-2 from recrystallization in methanol, as already pointed out), the DSC experiments were done with a sample of pure polymorph-2 and a sample containing a mixture of the two polymorphs obtained from recrystallization from methanol. The obtained DCS heating curves are shown in Figure 7.

As seen in the figure, the pure sample of polymorph-2 exhibits an endothermic peak at 176.2 ± 0.8 °C, with an enthalpy of fusion of 36.4 ± 1.0 kJ mol^{-1}, which corresponds to the melt of this polymorph. In the curve of the sample containing the mixture of the two polymorphs, the melting of polymorph-2 is also observed as a first endothermic process, followed by a

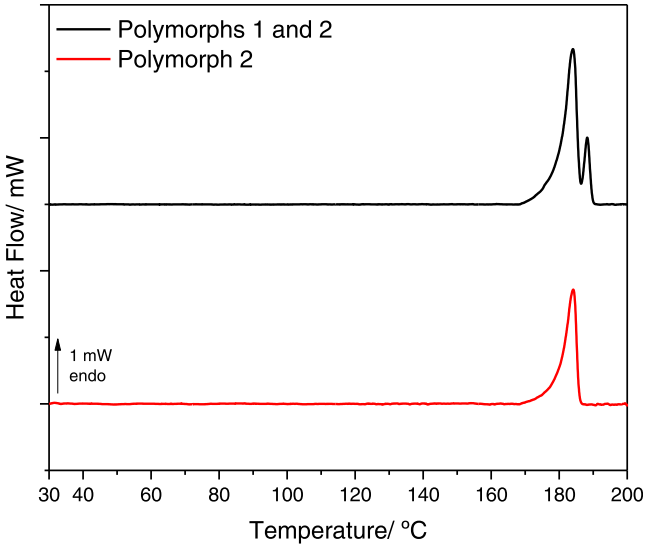

Figure 7. DSC heating curves of two samples of ROY-ol, one corresponding to pure polymorph-2 and the other to a mixture of polymorphs 1 and 2 (heating rate: 10 °C min^{-1}; masses: 0.85 mg, polymorph-1 + polymorph-2 mixed sample; 0.8 mg, pure polymorph-2 sample).

second melting process, which takes place at 187 °C. It was tempting to ascribe the second melting peak to the melting of polymorph-1, but, as shown below, the reality is considerably more complex.

Since low-enthalpy processes occurring before the melting processes are frequently undetectable in DSC experiments (in particular, when they take place in a wide range of temperatures), and also because we wanted to observe the thermal behavior of polymorph-1 as an isolated species, the two polymorphs of ROY-ol were subjected to investigation by PLTM.

In the PLTM analysis of polymorph-2, which is illustrated in Figure 8, the only visible thermodynamic event was, as suggested by the DSC data, the melting of the crystal, starting at 165 °C and finishing at 187 °C, in accordance with the DSC information recorded for the sample of this polymorph.

https://doi.org/10.1021/acs.cgd.2c00462
Cryst. Growth Des. 2022, 22, 5375−5389

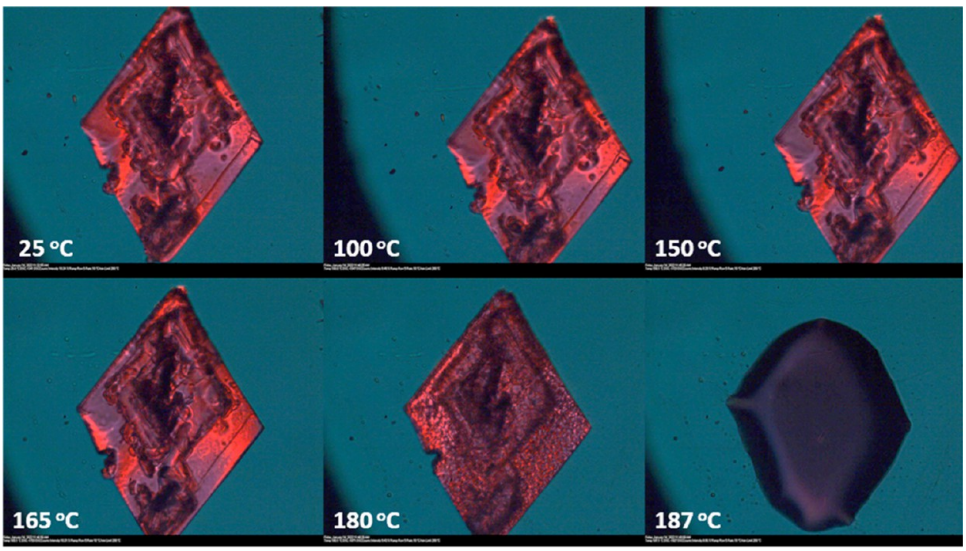

Figure 8. PLTM images obtained along the heating of a crystal of the polymorph-2 of ROY-ol (heating rate: 10 °C min^{-1}).

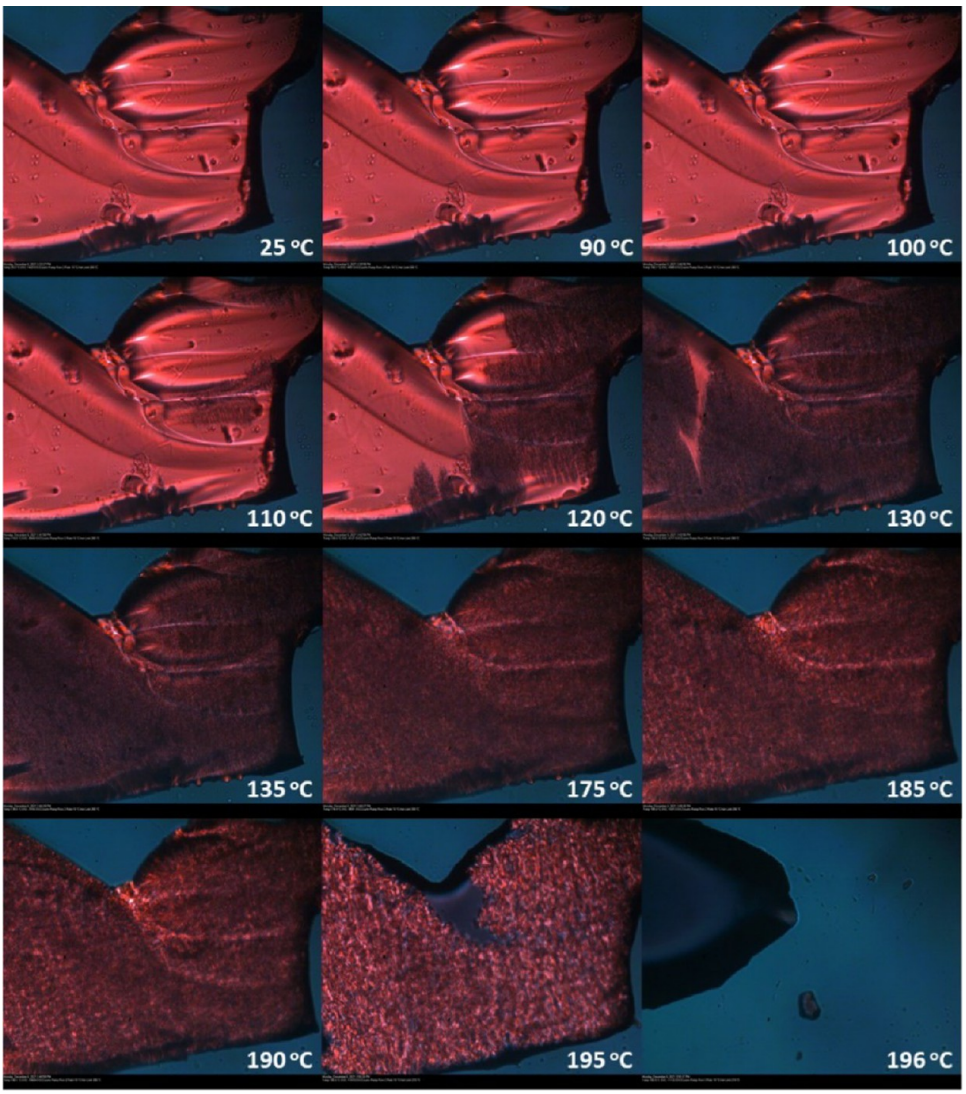

Figure 9. PLTM images obtained along the heating of a crystal of the polymorph-1 of ROY-ol (heating rate: 10 °C min^{-1}). These pictures were extracted from the PLTM video submitted as the Supporting Information.

https://doi.org/10.1021/acs.cgd.2c00462
Cryst. Growth Des. 2022, 22, 5375−5389

On the other hand, in the PLTM images of a crystal of polymorph-1 (Figure 9), one can clearly observe a solid−solid transition, from polymorph-1 to another solid form, which starts at ca. 100 °C and is completed at around 135 °C. After this transformation, the melting process starts at around 175 °C, with the first drops of the melted material being formed, as seen in the center of the image shown in Figure 9. At 196 °C, the melting of the whole sample is complete. The first steps of this latter transition are better observed in the PLTM video submitted as the Supporting Information. These results mean that, upon heating, polymorph-1 converts into a new polymorph that melts at higher temperatures than polymorph-2 (polymorph-3), and that the melting process observed at higher temperatures in the DSC experiments (see Figure 7, black curve) is not the melting of polymorph-1, but that of polymorph-3. The solid−solid transition between polymorph-1 and polymorph-3 is not detected in the DSC experiments because of the broad range of temperatures where it occurs and presumably also because of its low enthalpy.

This solid−solid transition between polymorphs 1 and 3 was also investigated by temperature-variation Raman spectroscopy, where the same temperature-variation program used in the PLTM experiment was applied. Monitoring of the optical image of the crystal selected for the Raman experiments at the microscope was concordant with the results of PLTM, with observation of changes in the morphology of the crystal compatible with the solid−solid transition, including its color that changes from bright-burgundy to dark-burgundy. The Raman spectra obtained before and after the solid−solid transition are presented in Figure 10.

As seen in Figure 10, the Raman spectrum of polymorph-3 is clearly distinct from that of polymorphs 1 and 2, in particular in the low-frequency region. This spectral region is in general more sensitive to rearrangements of the intermolecular environment than the higher-frequency spectroscopic regions, which are more related to the structure of individual molecules in the crystal. Nevertheless, also in the higher-frequency region (above 1300 cm^{-1}), the Raman spectrum of polymorph-3 of ROY-ol is rather distinct from those of polymorphs 1 and 2 of the compound. Particularly noticeable are the intense bands at 99 and 60 cm^{-1} appearing in the spectrum of polymorph-3, which can act as marker bands of this form. In addition, the most intense band of the Raman spectra of all polymorphs, which appears in the spectra of both polymorphs 1 and 2 at 816 cm^{-1}, is observed at 812 cm^{-1} in the case of polymorph-3.

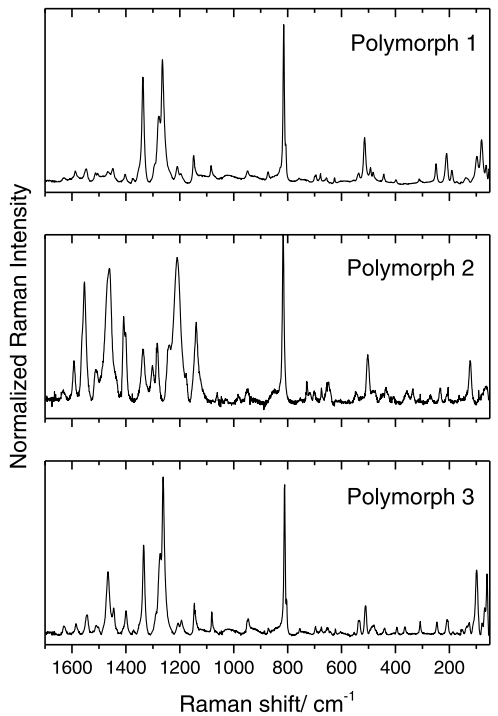

Figure 10. Raman spectra of ROY-ol polymorphs 1, 2, and 3 in the 50−1700 cm^{-1} Raman shift range.

In some samples, the optically isotropic material, amorphous ROY, could be identified. Being isotropic, the amorphous material was clearly in the images obtained using crossed polarizers (see Figure S13), where it is not distinguishable from the black background. In some PLTM experiments, an interesting thermal behavior was observed. Figure 11 shows the heating of a crystal of polymorph-2 with a small amount of this amorphous material on it. As seen in this figure (see also PLTM Video S2 submitted as the Supporting Information), crystallization of the isotropic material starts at approximately 80 °C. The formed crystalline material then melts at ca. 150 °C, which is a melting temperature that does not correspond to those of either polymorph-2 or polymorph-3. This crystalline phase is most likely not also polymorph-1, as in all experiments carried out on form 1, at the same scanning rate, a solid−solid transition to polymorph-3 was always observed, starting at ca. 100 °C. The existence of another ROY-ol polymorph (polymorph-4; also dark-burgundy) is then proposed. Unfortunately, further characterization of this polymorph was not yet possible, considering that its generation proved to be very difficult to control. Indeed, the formation of the amorphous phase (which was the precursor of polymorph-4 in our experiments) from the melted compound is not possible because decomposition takes place immediately after melting, while the generation of the amorphous material using the solvent evaporation method was found to be fortuitous and, when it is observed, it constitutes only a residual fraction of the obtained material.

3.4. DFT Calculations for the Isolated Molecule (ROY-ol vs AcROY vs ROY): Correlating the Intramolecular Potentials for Internal Rotation about the N−$C_{(thiophene)}$ Bond and Polymorphism. As observed before for ROY, AcROY, and other similar molecules bearing an NH bridging group (connecting two ring moieties) in the ortho-position to a nitro substituent in a phenyl ring,[1,5−17] the low-energy conformers of the isolated ROY-ol molecule have an intramolecular H-bond established between the NH bridging group and the *ortho*-nitro group. This structural characteristic limits the conformational space of this type of molecule and gives exceptional relevance to other internal degrees of conformational flexibility. A search on the DTF(B3LYP)/6-311++G(2d,p) potential energy surface of ROY-ol allowed to identify four distinct low-energy conformers of the molecule, which are represented in Figure 12. Conformer A is the most stable one, followed by conformers B, C, and D, which are predicted to be 1.4, 3.5, and 4.3 kJ mol^{-1} higher in energy than A, respectively. The conformers differ in the orientation of the OH substituent present in the nitrophenyl ring (which may exist in two stable arrangements, pointing toward the nitro group, in A and B forms, or against this group, in C and D forms) and/or in the relative orientation of the two rings (with the cyano group pointing to the side of the nitro group, in B and D forms, or to

https://doi.org/10.1021/acs.cgd.2c00462
Cryst. Growth Des. 2022, 22, 5375−5389

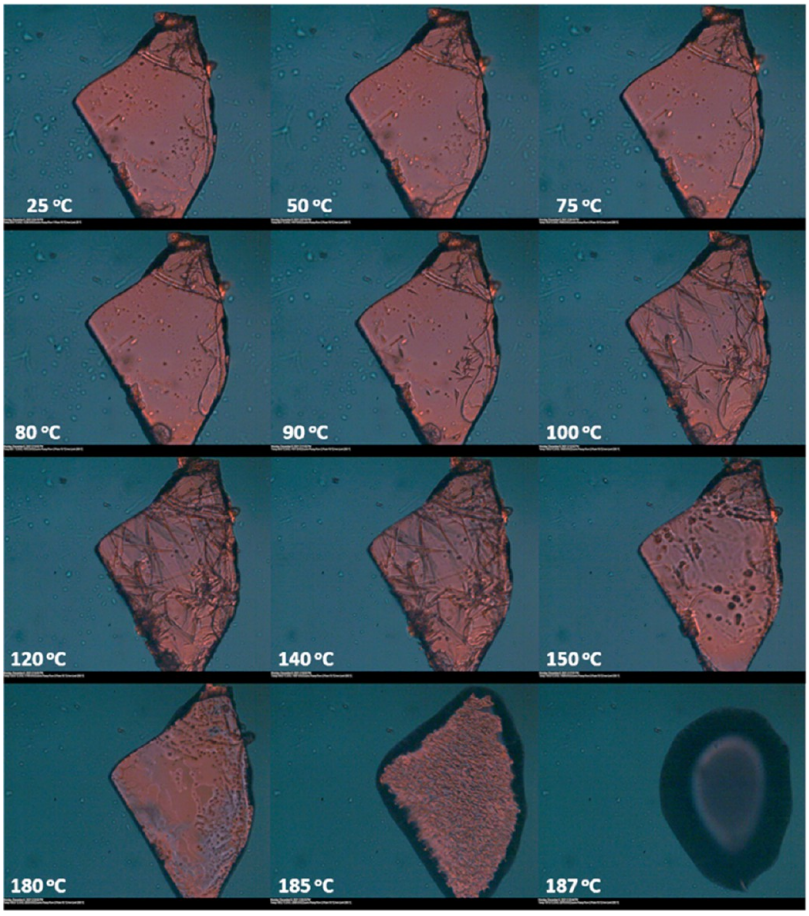

Figure 11. PLTM images obtained along the heating of the ROY-ol amorphous material on a crystal of polymorph-2 (heating rate: 10 °C min^{-1}). The PLTM Video S2, submitted as the Supporting Information, shows the entire experiment.

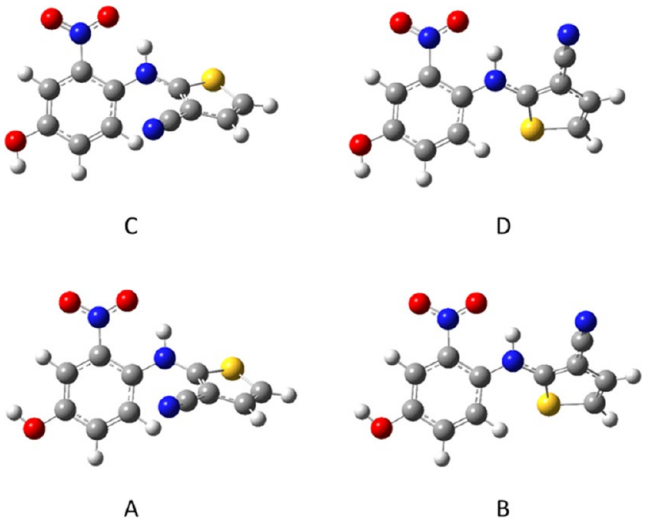

Figure 12. Geometries of the four low-energy conformers of ROY-ol. Each of the represented structures has a symmetry-equivalent form.

the opposite direction, in A and C forms), and all conformers have a symmetry-equivalent form.

The C−N−C−S dihedral angle values in conformers A to D are, by this order, 126.2, 35.1, 129.8, and 33.9°. Interestingly, the highest-energy conformer of the isolated molecule of ROY-ol (conformer D) is the one existing in both polymorphs 1 and 2 of the compound. In polymorph-1, the C−N−C−S dihedral angle is −31.6°, i.e., the conformation assumed by the molecule in the crystal is very much close to that of isolated conformer D. On the other hand, in polymorph-2, the C−N−C−S dihedral angle in the two different molecules in the asymmetric unit is −6.7(5) and 7.9(5)°, i.e., in this crystal, the molecules correspond to a strongly distorted conformer D where the two rings are almost coplanar.

Like in the previously studied analogue molecules, the most relevant torsional coordinate in terms of its impact on the optical properties of the ROY-ol molecule is precisely defined by the $N-C_{(thiophene)}$ bond (θ in Scheme 1, related to the C−N−C−S dihedral angle), which determines in a large amount the extension of the π-electron delocalization in the molecule. When the two rings are coplanar, the π-electron delocalization reaches its maxima and the energy gap between the ground and excited electronic states reaches its minimum values. In the case of ROY and the known ROY derivatives,[1,6−17] the general rule is that for small angles between the two ring planes, the maximum of absorption appears in the green region of the electromagnetic spectrum, so that the compound appears in tones of red/burgundy, while large angles between the ring planes lead to shift the absorption maximum to the blue, and the compound appears in yellow. For intermediate values of the angle between the two ring planes, the compound is perceived as orange. The $N-C_{(thiophene)}$ torsional coordinate is also known to be quite flexible, with low-energy barriers separating the conformers that differ in the spatial arrangement of this bond. For example, in the case of ROY-ol, the lowest-energy barrier separating conformers A and

https://doi.org/10.1021/acs.cgd.2c00462
Cryst. Growth Des. 2022, 22, 5375−5389

B has a height of only 2.9 kJ mol^{-1} when taken in the A → B direction (1.5 kJ mol^{-1} in the opposite direction), according to the performed DFT calculations, and that between conformers C and D is similar (3.0 kJ mol^{-1} in the C → D direction; 2.2 kJ mol^{-1} in the reverse direction). The low-energy barriers, together with the small energy differences between the conformers, justify the fact that different conformers have been found to be present as structural units of the different polymorphs of this type of compound, noteworthy in the case of the parent ROY compound.[1,6−12]

The barrier to internal rotation of the OH group of ROY-ol, which leads to interconversion between the pairs of conformers A and C, on the one side, and B and D, on the other side, are comparatively higher than those associated with the rotamerization about the N−C$_{(thiophene)}$ bond. Nevertheless, they are still small in absolute terms, with the A → C barrier predicted by the calculations being 14.1 kJ mol^{-1} (10.7 kJ mol^{-1} in the reverse direction) and that associated with the B → D transformation being 12.2 kJ mol^{-1} (9.3 kJ mol^{-1} in the opposite direction).

Figure 13 shows the calculated potential energy profile for internal rotation around the N−C$_{(thiophene)}$ bond in the isolated molecule of ROY-ol, as defined by the C−N−C−S dihedral angle. The corresponding potential energy profiles for ROY and AcROY have also been calculated and are plotted in the figure, for comparison. Symbols representing the different polymorphs of the three compounds are superposed to the corresponding energy curves, with their color representing the color of the polymorph (classified in a simple way only as red, orange, and yellow). The symbols are placed at the values of the C−N−C−S dihedral angle observed in the crystals (see Table S3, in the Supporting Information; for crystals with more than one molecule in the asymmetric unit, as in the case of polymorph-2 of ROY-ol, the value of the dihedral angle in the different molecules is indicated, so that the symbol corresponding to these polymorphs appears repeated in the plot).

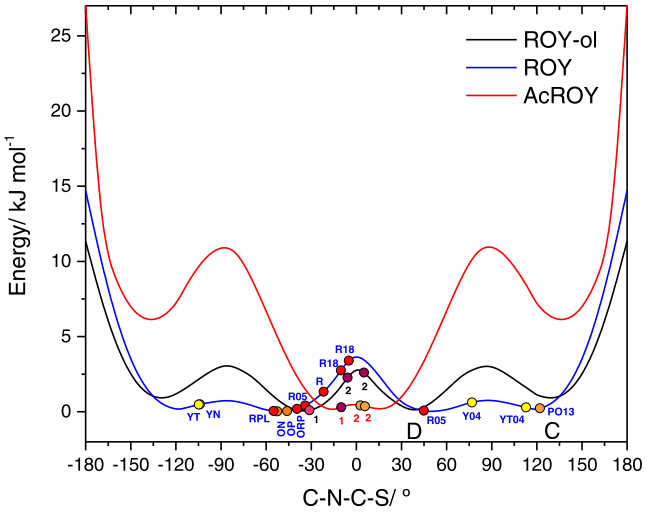

Figure 13. DFT-calculated potential energy profiles (gas phase) associated with the internal rotation θ, as defined by the dihedral angle C−N−C−S, for ROY-ol, AcROY, and ROY compounds, and corresponding dihedral angles observed experimentally for the different polymorphs (indicated by the circles, colored according to the color of the polymorph). See the text for details. In the case of ROY polymorphs YN, YT, YT04, and PO13, whose C−N−C−S dihedral angle is larger than 90°, the angles between the planes of the ring correspond to the absolute value of the difference between 180° and the value of the dihedral angle, i.e., 76.0, 75.3, 67.2, and 57.9°, the latter value thus being similar to those found for the remaining orange polymorphs of ROY. The exceptions to the "color vs. angle between the ring planes" general rule are only the RPL red polymorph of ROY, whose angle stays in the range of those appearing in the orange polymorphs of the compound, and the orange polymorph-2 of AcROY, whose angle stays in the range observed for red/burgundy polymorphs..

The calculation of the potential energy curves for internal rotation around the N−C$_{(thiophene)}$ bond in ROY and its derivatives is known to pose some difficulties, in particular because of the coupling of the θ coordinate with other coordinates (e.g., inversion at the bridging nitrogen atom) and the need to tread adequately the π electron delocalization. To deal with the first problem, which appears particularly relevant in the $\theta = \pm(120-180°)$ ranges (i.e., near the position of the most hindered, highest-energy transition state; see Figure 13), the scans shown in Figure 13 were done in this region point by point (instead of in the continuous mode, where the final geometry of a given point is used as a basis to the starting geometry of the next point along the scan), with the starting geometry at each point possessing the two rings (and corresponding substituents) as well as the amine bridging group strictly planar. The questions related to the treatment of the π-electron delocalization, on the other hand, have been addressed previously by several authors, in the case of the parent ROY molecule in the context of polymorph relative energy prediction,[36−39] and the ability of DFT methods to deal properly with this property has been questioned, but the best theoretical approach to be used for calculating the intrinsic potential energy profile defined by θ is still under debate, considering that no experimental data is available for the isolated molecule of the compound and benchmark of the different methods with other theoretical approaches is not straightforward for calculation of relative conformational energies. In any case, the calculations performed in the present study can be expected to be at least qualitatively appropriate for a comparison of the global energy profiles of ROY-ol, ROY, and AcROY.

As can be seen in Figure 13, the scan profiles of the three compounds are, as expected, similar. However, it is interesting to note that the flatness of the potential energy profiles in the relevant potential energy region, defined by values of the C−N−S−C dihedral angle ranging from about −120° to +120°, correlates with the number of polymorphs identified for the three compounds hitherto. According to the performed calculations, the profile for ROY is that exhibiting the lowest-energy barriers in the relevant potential energy region, this compound having the largest number of known polymorphs, while ROY-ol, with four different polymorphs reported in the present study, has intermediate energy barriers, and AcROY, with only two polymorphs discovered until now, has the potential energy curve with the highest barriers among the three compounds. This correlation between the relative flatness of the potential energy profiles in the three compounds and the number of polymorphs discovered for each one seems to be significant because it can be expected that if less energy is required to adjust the structure of individual molecules to specific packing requirements the number of energy-accessible stable crystalline structures should tend to be larger.

Lower-energy intrinsic torsional barriers may also be correlated to the accessibility of polymorphs where the structural molecular unit is composed of a different conformer. In accordance with this conclusion, and as depicted in Figure 13, among the three molecules now being compared, ROY exhibits

https://doi.org/10.1021/acs.cgd.2c00462
Cryst. Growth Des. 2022, 22, 5375−5389

4 polymorphs formed by one conformer and 8 polymorphs formed by a second conformer, and AcROY has 2 polymorphs formed by the same conformer. In the case of ROY-ol, both polymorphs 1 and 2 are composed of conformer D, but for polymorph-2, the molecule is strongly distorted compared to its geometry in the gas phase, as has been highlighted above. Moreover, the conformer(s) present in polymorphs 3 and 4 is(are) not known, since the determination of the structure of these two polymorphs was not yet undertaken. In the case of polymorph-3, since it can be easily obtained from polymorph-1 without requiring a large amount of energy and also because it is formed in a process that does not require destruction of the crystals (as shown in the PLTM experiments described in Section 3.3), it can be expected that conformer D is also present in this polymorph (to be confirmed). On the other hand, no clues on the nature of the constituting conformer of polymorph-4 can be extracted from the experiments performed in our investigation, so this stays a completely open question to further investigation.

4. CONCLUSIONS

In this study, the color polymorphism in ROY-ol, a novel member of the ROY family of compounds, has been investigated. In total, four polymorphs were identified, with polymorph-1 being bright-burgundy and polymorphs 2, 3, and 4 dark-burgundy. The crystal structures of polymorphs 1 and 2 were determined by single-crystal XRD, both forms being monoclinic, space group $P2_1/n$ (no. 14), with a = 7.867(2), b = 13.046(3), c = 11.519(4) Å, β = 107.26(3)°, V = 1129.0(6) Å^3, Z = 4, and Z' = 1 for polymorph-1 and a = 8.6557(7), 12.9351(12), 20.2404(18) Å, β = 90.806(4), V = 2265.9(3) Å^3, Z = 8, and Z' = 2 for polymorph-2.

In the crystals, the molecular conformation of the molecules differs significantly, as well as the hydrogen-bonding network. In the case of polymorph-1, the molecules exist in a conformation very closely resembling that of the conformer D predicted for the gas phase, thus having a significant deviation from planarity, with the C−N−C−S dihedral angle being −31.6(3)° (similar to that of conformer D for the isolated molecule: ±33.9°). In polymorph-1, the nitro group is also significantly tilted (23.1(2)°) from the plane of the phenyl ring. On the other hand, in polymorph-2, both symmetry-independent molecules are almost strictly planar, with the C−N−C−S dihedral angle being −6.7(5)° in one of the molecules and 7.9(5)° in the other. The conformation of the molecules is still related to that of conformer D for the isolated molecule but is strongly disturbed due to intermolecular interactions.

In both polymorphs 1 and 2, a strong N−H···O hydrogen bond between the cyano and hydroxyl groups of neighbor molecules exists, which plays a major structural role in the crystal. Another common structural element of both polymorphs is the fact that one of the O atoms of the nitro group does not participate in the hydrogen-bond network. However, the additional intermolecular interactions are distinct and result in markedly different tridimensional arrangements. Short contacts were found to be more abundant in polymorph-1, while the sum of the fractional areas assigned to the principal hydrogen-bond-related contacts (H···O/O···H, H···N/N···H, and H···S/S···H) in the Hirshfeld analysis (d_{norm} maps on the Hirsfeld surface) suggests that H-bonding interactions are globally more relevant in the packing of polymorph-2 than in polymorph-1. Polymorphs 1 and 2 were also characterized vibrationally by infrared and Raman spectroscopies, supported by fully periodic density functional theory (DFT) calculations, which allowed for spectra assignment. Marker bands for fast identification of the polymorphs were proposed.

The performed thermal analysis studies, undertaken by DSC, PLTM, and temperature-variation Raman spectroscopy, allowed to identify one additional polymorph of ROY-ol (polymorph-3). Polymorph-3 is formed upon heating of polymorph-1, via a solid−solid, low-enthalpy, transition that starts at ca. 100 °C and is completed at around 135 °C, at a 10 °C min^{-1} scanning rate. Raman marker bands for fast spectroscopic identification of this polymorph were also offered. An additional polymorphic form, polymorph-4, is proposed, which melts at about 150 °C, and was obtained upon recrystallization of the amorphous material upon heating (at about 80 °C).

Investigation of the conformational space of the isolated ROY-ol molecule within the DFT framework (together with similar calculations on ROY and AcROY) allowed to establish a "color of the polymorph vs. angle between the ring planes" empirical rule, while the global profile of the potential energy curves related to the C−N−C−S torsional coordinate in the molecules belonging to the ROY family was also correlated to the trend of the compound to form polymorphs; the more flat the torsional potential in the relevant potential energy region, defined by values of the C−N−S−C dihedral angle ranging from about −120 to +120°, the higher the number of easily accessible polymorphs.

As a whole, in this study, a detailed description of the color polymorphism exhibited by ROY-ol has been performed, which is an additional contribution to the understanding of this phenomenon, in particular in what concerns the captivating ROY family of compounds.

■ ASSOCIATED CONTENT

Supporting Information

The Supporting Information is available free of charge at https://pubs.acs.org/doi/10.1021/acs.cgd.2c00462.

Figures S1−S6, with the ^{1}H and ^{13}C NMR and IR spectra of 4-benzyloxy-1-fluoro-2-nitrobenzene, 2-((4-benzyloxy-2-nitrophenyl)amino)thiophene-3-carbonitrile, and ROY-ol; Figure S7, with the visible absorption spectrum of polymorph-2 and the position of the color obtained from this spectrum in the CIE color map; Figures S8−S9, with the comparison between the DFT-calculated IR and Raman spectra for polymorphs 1 and 2 and the corresponding experimental spectra; Figures S10−S12, with the results of Hirshfeld analysis; Figure S13, with polarized light and cross-polarized light photographs of a sample showing small crystals of polymorph-2 and an amount of amorphous ROY-ol; Tables S1−S2, with observed infrared and Raman bands of ROY-ol polymorphs 1 and 2 and their respective DFT-calculated frequencies, with proposed assignments; Table S3, with C−N−C−S dihedral angles in the different polymorphs of ROY, AcROY, and ROY-ol (PDF)

Crystallographic data tables, with the structural X-ray data for ROY-ol polymorphs 1 and 2 (PDF)

PLTM video, showing the transformation of polymorph-1 into polymorph-3 (Video S1) (AVI)

PLTM2 video, showing formation of polymorph-4 (Video S2) (AVI)

https://doi.org/10.1021/acs.cgd.2c00462
Cryst. Growth Des. 2022, 22, 5375−5389

Accession Codes

CCDC 2160983−2160984 contain the supplementary crystallographic data for this paper. These data can be obtained free of charge via www.ccdc.cam.ac.uk/data_request/cif, or by emailing data_request@ccdc.cam.ac.uk, or by contacting The Cambridge Crystallographic Data Centre, 12 Union Road, Cambridge CB2 1EZ, UK; fax: +44 1223 336033.

CIF files containing the supporting crystallographic data were deposited at the Cambridge Crystallographic Data Centre, with references CCDC 2160983 (polymorph-1) and 2160984 (polymorph-2).

AUTHOR INFORMATION

Corresponding Author

Bernardo A. Nogueira − *CQC-IMS, Department of Chemistry, University of Coimbra, P-3004-535 Coimbra, Portugal; CMIC, Dipartimento di Chimica, Materiali e Ingegneria Chimica "G. Natta", Politecnico di Milano, 20133 Milano, Italy;* orcid.org/0000-0002-1756-377X; Email: ban@qui.uc.pt

Authors

Susana M. M. Lopes − *CQC-IMS, Department of Chemistry, University of Coimbra, P-3004-535 Coimbra, Portugal;* orcid.org/0000-0002-1580-5667

Alberto Milani − *CMIC, Dipartimento di Chimica, Materiali e Ingegneria Chimica "G. Natta", Politecnico di Milano, 20133 Milano, Italy;* orcid.org/0000-0001-6026-5455

Vânia André − *Centro de Química Estrutural-IMS, Instituto Superior Técnico, Universidade de Lisboa, 1049-001 Lisboa, Portugal;* orcid.org/0000-0001-5599-8355

José A. Paixão − *CFisUC, Department of Physics, University of Coimbra, P-3004-516 Coimbra, Portugal;* orcid.org/0000-0003-4634-7395

M. Ermelinda S. Eusébio − *CQC-IMS, Department of Chemistry, University of Coimbra, P-3004-535 Coimbra, Portugal;* orcid.org/0000-0002-5515-7721

Teresa M. V. D. Pinho e Melo − *CQC-IMS, Department of Chemistry, University of Coimbra, P-3004-535 Coimbra, Portugal;* orcid.org/0000-0003-3256-4954

M. Teresa Duarte − *Centro de Química Estrutural-IMS, Instituto Superior Técnico, Universidade de Lisboa, 1049-001 Lisboa, Portugal;* orcid.org/0000-0003-0994-1352

Chiara Castiglioni − *CMIC, Dipartimento di Chimica, Materiali e Ingegneria Chimica "G. Natta", Politecnico di Milano, 20133 Milano, Italy;* orcid.org/0000-0002-6945-9157

Rui Fausto − *CQC-IMS, Department of Chemistry, University of Coimbra, P-3004-535 Coimbra, Portugal;* orcid.org/0000-0002-8264-6854

Complete contact information is available at: https://pubs.acs.org/10.1021/acs.cgd.2c00462

Author Contributions

B.A.N. conceptualized the study, wrote a preliminary version of the manuscript, and participated in most of the experimental work and in theoretical studies. R.F. contributed to the conceptualization of the study, took responsibility for supervision and data analysis, and wrote the final draft of the manuscript. S.M.M.L. and T.M.V.D.P.e.M. were responsible for the development of the synthetic route and its implementation. M.E.S.E. participated in the design of the DSC studies and in the writing of the corresponding section of the manuscript. A.M. and C.C. performed the fully periodic DFT calculations. V.A., M.T.D., and J.A.P. performed the XRD studies and wrote the corresponding section of the manuscript. All authors have participated in the discussion of the results and agreed with the final version of the manuscript.

Notes

The authors declare no competing financial interest.

ACKNOWLEDGMENTS

The CQC-IMS is financially supported by the Portuguese Science Foundation ("Fundação para a Ciência e a Tecnologia", FCT), Projects CQC UIDB/00313/2020 and UIDP/00313/2020, and CQE-IMS is funded by UIDB/00100/2020, UIDP/00100/2020, and LA/P/0056/2020 (National Funds). CFisUC is funded by FCT through the projects UIDB/04564/2020 and UIDP/04564/2020. The authors also want to acknowledge Roberto Dovesi, Fabien Pascale, Michel Rerat, and Matteo Tommasini for their help in solving some technical problems related to the periodic calculations. Access to instruments from Laser-Lab Coimbra, the Nuclear Magnetic Resonance Laboratory of CQC-IMS (www.nmrccc.uc.pt), and TAIL-UC (ICT_2009_02_012_1890) facilities (funded under QREN-Mais Centro) is gratefully acknowledged. B.A.N. also acknowledges FCT for the SFRH/BD/129852/2017 Ph.D. Scholarship. V.A. acknowledges FCT for a contract under CEECIND program: CEECIND/00283/2018.

REFERENCES

(1) Nogueira, B. A.; Castiglioni, C.; Fausto, R. Color Polymorphism in Organic Crystals. *Commun. Chem.* **2020**, *3*, No. 34.

(2) Gentili, D.; Gazzano, M.; Melucci, M.; Jones, D.; Cavallini, M. Polymorphism as an Additional Functionality of Materials for Technological Applications at Surfaces and Interfaces. *Chem. Soc. Rev.* **2019**, *48*, 2502−2517.

(3) Cavallini, M.; Calò, A.; Stoliar, P.; Kengne, J. C.; Martins, S.; Matacotta, F. C.; Quist, F.; Gbabode, G.; Dumont, N.; Geerts, Y. H.; Biscarini, F. Liquid-Crystal Patterning: Lithographic Alignment of Discotic Liquid Crystals: A New Time-Temperature Integrating Framework. *Adv. Mater.* **2009**, *21*, 4688−4691.

(4) Gentili, D.; Durso, M.; Bettini, C.; Manet, I.; Gazzano, M.; Capelli, R.; Muccini, M.; Melucci, M.; Cavallini, M. A Time-temperature Integrator Based on Fluorescent and Polymorphic Compounds. *Sci. Rep.* **2013**, *3*, No. 2581.

(5) Lin, Z.; Mei, X.; Yang, E.; Li, X.; Yao, H.; Wen, G.; Chien, C.-T.; Chow, T. J.; Ling, Q. Polymorphism-dependent Fluorescence of Bisthienylmaleimide with Different Responses to Mechanical Crushing and Grinding Pressure. *CrystEngComm* **2014**, *16*, 11018−11026.

(6) Stephenson, G. A.; Borchardt, T. B.; Byrn, S. R.; Bowyer, J.; Bunnell, C. A.; Snorek, S. V.; Yu, L. Conformational and Color Polymorphism of 5-Methyl-2-[(2-nitrophenyl)amino]-3-thiophenecarbonitrile. *J. Pharm. Sci.* **1995**, *84*, 1385−1386.

(7) Yu, L.; Stephenson, G. A.; Mitchell, C. A.; Bunnell, C. A.; Snorek, S. V.; Bowyer, J. J.; Borchardt, T. B.; Stowell, J. G.; Byrn, S. R. Thermochemistry and Conformational Polymorphism of a Hexamorphic Crystal System. *J. Am. Chem. Soc.* **2000**, *122*, 585−591.

(8) Chen, S.; Guzei, I. A.; Yu, L. New Polymorphs of ROY and New Record for Coexisting Polymorphs of Solved Structures. *J. Am. Chem. Soc.* **2005**, *127*, 9881−9885.

(9) Tan, M.; Shtukenberg, A. G.; Zhu, S.; Xu, W.; Dooryhee, E.; Nichols, S. M.; Ward, M. D.; Kahr, B.; Zhu, Q. ROY Revisited, Again: The Eighth Solved Structure. *Faraday Discuss.* **2018**, *211*, 477−491.

(10) Gushurst, K. S.; Nyman, J.; Boerrigter, S. X. M. The PO13 Crystal Structure of ROY. *CrystEngComm* **2019**, *21*, 1363−1368.

(11) Tyler, A. R.; Ragbirsingh, R.; McMonagle, C. J.; Waddell, P. G.; Heaps, S. E.; Steed, J. W.; Thaw, P.; Hall, M. J.; Probert, M. R.

Encapsulated Nanodroplet Crystallization of Organic-Soluble Small Molecules. *Chem* **2020**, *6*, 1755−1765.
(12) Li, X.; Ou, X.; Rong, H.; Huang, S.; Nyman, J.; Yu, L.; Lu, M. The Twelfth Solved Structure of ROY: Single Crystals of Y04 Grown from Melt Microdroplets. *Cryst. Growth Des.* **2020**, *20*, 7093−7097.
(13) Li, H.; Stowell, J. G.; Borchardt, T. B.; Byrn, S. R. Synthesis, Conformational Polymorphism, and Construction of a G-T Diagram of 2-[(2Nitrophenyl)amino]-3-thiophenecarbonitrile. *Cryst. Growth Des.* **2006**, *6*, 2469−2474.
(14) He, X.; Griesser, U. J.; Stowell, J. G.; Borchardt, T. B.; Byrn, S. R. Conformational color Polymorphism and Control of Crystallization of 5-Methyl-2-[(4-methyl-2-nitrophenyl)amino]-3-thiophenecarbonitrile. *J. Pharm. Sci.* **2001**, *90*, 371−388.
(15) Lutker, K. M.; Tolstyka, Z. P.; Matzger, A. J. Investigation of a Privileged Polymorphic Motif: a Dimeric ROY Derivative. *Cryst. Growth Des.* **2008**, *8*, 136−139.
(16) Lévesque, A.; Maris, T.; Wuest, J. D. ROY Reclaims Its Crown: New Ways to Increase Polymorphic Diversity. *J. Am. Chem. Soc.* **2020**, *142*, 11873−11883.
(17) Nogueira, B. A.; Carvalho, M.; Paixão, J. A.; Eusébio, M. E. S.; Lopes, S. M. M.; Pinho e Melo, T. M. V. D.; Fausto, R. Portrayal of the Color Polymorphism in the 5-Acetyl-derivative of ROY. *CrystEngComm* **2022**, *24*, 1459−1474.
(18) Sheldrick, G. M. Crystal Structure Refinement with SHELXL. *Acta Crystallogr., Sect. C: Struct. Chem.* **2015**, *71*, 3−8.
(19) Sheldrick, G. M. SHELXT − Integrated Space-Group and Crystal-Structure Determination. *Acta Crystallogr., Sect. A: Found. Adv.* **2015**, *71*, 3−8.
(20) Frisch, M. J.; Trucks, G. W.; Schlegel, H. B.; Scuseria, G. E.; Robb, M. A.; Cheeseman, J. R.; Scalmani, G.; Barone, V.; Mennucci, B.; Petersson, G. A.et al. *Gaussian 09*, revision D.01; Gaussian, Inc.: Wallingford, CT, 2009.
(21) Becke, A. D. Density-functional Exchange-energy Approximation with Correct Asymptotic Behavior. *Phys. Rev. A* **1988**, *38*, 3098−3100.
(22) Lee, C.; Yang, W.; Parr, R. G. Development of the Colle-Salvetti Correlation-energy Formula into a Functional of the Electron Density. *Phys. Rev. B* **1988**, *37*, 785−789.
(23) McLean, A. D.; Chandler, G. S. Contracted Gaussian Basis Sets for Molecular Calculations. I. Second Row Atoms, Z = 11−18. *J. Chem. Phys.* **1980**, *72*, 5639−5648.
(24) Dovesi, R.; Erba, A.; Orlando, R.; Zicovich-Wilson, C. M.; Civalleri, B.; Maschio, L.; Rérat, M.; Casassa, S.; Baima, J.; Salustro, S.; Kirtman, B. Quantum-mechanical Condensed Matter Simulations with CRYSTAL. *Wiley Interdiscip. Rev. Comput. Mol. Sci.* **2018**, *8*, No. e1360.
(25) Dovesi, R.; Saunders, V. R.; Roetti, C.; Orlando, R.; Zicovich-Wilson, C. M.; Pascale, F.; Civalleri, B.; Doll, K.; Harrison, N. M.; Bush, I. J.; D'Arco, P.; Llunell, M.; Causà, M.; Noël, Y.; Maschio, L.; Erba, A.; Rerat, M.; Casassa, S. *CRYSTAL17 User's Manual*; University of Torino, 2018.
(26) Adamo, C.; Barone, V. Toward Reliable Density Functional Methods without Adjustable Parameters: The PBE0 Model. *J. Chem. Phys.* **1999**, *110*, 6158−6170.
(27) Ditchfield, R.; Hehre, W. J.; Pople, J. A. Self-Consistent Molecular Orbital Methods. IX. Extended Gaussian-type basis for molecular-orbital studies of organic molecules. *J. Chem. Phys.* **1971**, *54*, 724−728.
(28) Merrick, J. P.; Moran, D.; Radom, L. An Evaluation of Harmonic Vibrational Frequency Scale Factors. *J. Phys. Chem. A* **2007**, *111*, 11683−11700.
(29) Spackman, M. A.; Byrom, P. G. A Novel Definition of a Molecule in a Crystal. *Chem. Phys. Lett.* **1997**, *267*, 215−220.
(30) Spackman, M. A.; Jayatilaka, D. Hirshfeld Surface Analysis. *CrystEngComm* **2009**, *11*, 19−32.
(31) Wolff, S. K.; Grimwood, D. J.; McKinnon, J. J.; Turner, M. J.; Jayatilaka, D.; Spackman, M. A. *Crystal Explorer17*, version 17.5; University of Western Australia: Crawley, 2017.
(32) McKinnon, J. J.; Mitchell, A. S.; Spackman, M. A. Hirshfeld Surfaces: A New Tool for Visualising and Exploring Molecular Crystals. *Chem.—Eur. J.* **1998**, *4*, 2136−2141.
(33) Spackman, M. A.; McKinnon, J. J. Fingerprinting Intermolecular Interactions in Molecular Crystals. *CrystEngComm* **2002**, *4*, 378−392.
(34) Rohl, A. L.; Moret, M.; Kaminsky, W.; Claborn, K.; McKinnon, J. J.; Kahr, B. Hirshfeld Surfaces Identify Inadequacies in Computations of Intermolecular Interactions in Crystals: Pentamorphic 1,8-Dihydroxyanthraquinone. *Cryst. Growth Des.* **2008**, *8*, 4517−4525.
(35) Parkin, A.; Barr, G.; Dong, W.; Gilmore, C. J.; Jayatilaka, D.; McKinnon, J. J.; Spackman, M. A.; Wilson, C. C. Comparing Entire Crystal Structures: Structural Genetic Fingerprinting. *CrystEngComm* **2007**, *9*, 648−652.
(36) Thomas, S. P.; Spackman, M. A. The Polymorphs of ROY: A Computational Study of Lattice Energies and Conformational Energy Differences. *Aust. J. Chem.* **2018**, *71*, 279−284.
(37) Nyman, J.; Yu, L.; Reutzel-Edens, S. Accuracy and Reproducibility in Crystal Structure Prediction: The Curious Case of ROY. *CrystEngComm* **2019**, *21*, 2080−2088.
(38) Greenwell, C.; McKinley, J. L.; Zhang, P.; Zeng, Q.; Sun, G.; Li, B.; Wen, S.; Beran, G. J. O. Overcoming the Difficulties of Predicting Conformational Polymorph Energetics in Molecular Crystals via Correlated Wavefunction Methods. *Chem. Sci.* **2020**, *11*, 2200−2214.
(39) Chen, Z.; Gui, Y.; Cui, K.; Schmit, J. R.; Yu, L. Prolific Polymorph Generator ROY in Its Liquid and Glass: Two Conformational Populations Mirroring the Crystalline-State Distribution. *J. Phys. Chem. B* **2021**, *125*, 10304−10311.

https://doi.org/10.1021/acs.cgd.2c00462
Cryst. Growth Des. 2022, 22, 5375−5389